Article

The Life and Death of the Hiatus Consistently Explained

Kristoffer Rypdal [1]

[1] Department of Mathematics and Statistics, UiT–The Arctic University of Norway; kristoffer.rypdal@uit.no

Abstract: The main features of the instrumental global mean surface temperature (GMST) are reasonably well described by a simple linear response model driven by anthropogenic, volcanic and solar forcing. This model acts as a linear long-memory filter of the forcing signal. The physical interpretation of this filtering is the delayed response due to the thermal inertia of the ocean. This description is considerably more accurate if El Niño Southern Oscillation (ENSO) and the Atlantic Multi-decadal Oscillation (AMO) are regarded as additional forcing of the global temperature and hence subject to the same filtering as the other forcing components. By considering these as predictors in a linear regression scheme, more than 92% of the variance in the instrumental GMST over the period 1870-2017 is explained by this model, and in particular all features of the 1998 – 2015 hiatus, including its death. While the more prominent pauses during 1870 – 1915 and 1940 – 1970 can be attributed to clustering in time of strong volcanic eruptions, the recent hiatus is an unremarkable phenomenon that is attributed to ENSO and a small contribution from solar activity.

Keywords: hiatus; attribution; volcanic forcing; solar forcing; anthropogenic forcing; AMO; ENSO; multiple regression; long-memory response

---

1. Introduction

According to instrumental observations [8] the global mean surface temperature (GMST) has risen at increasing rate throughout the instrumental period 1850 – 2017 Common Era (CE). This rise, however, has been interrupted by three pauses of no, or even negative, growth. These are the periods 1870 – 1915, 1940 – 1970, and 1998 – 2015. The last hiatus is the shortest and least spectacular of these, and the reason for the great attention it has received is primarily that it is the first pause observed since global warming became a scientific and political issue in the 1980s.

Multiple, linear regression has been applied to explain the GMST satellite record for the period 1979 – 2011 CE by foster and Rahmstorf (2011) [1]. Their emphasis was on eliminating the effects of volcanic and solar forcing, and the El Niño Southern Oscillation (ENSO), to recover the anthropogenic trend in the data. Lean and Rind (2008) [2] apply such regression with the volcanic, solar, and anthropogenic, forcing signals, and in addition the multivariate ENSO index, as predictors for the instrumental GMST for the period 1889 – 2006. This description captures the initial part of the hiatus for the period 1998 – 2006, but not the pauses during the intervals 1870 – 1915 and 1940 – 1970. Rypdal (2015) [3] applies a long-range memory (LRM) response filter to the forcing and introduces the Atlantic Multidecadal Oscillation (AMO) index as a predictor in addition to the Niño3.4 index. This approach explains 89% of the variance of the 1880 – 2010 GMST and captures all three pauses.

The main purpose of the present paper is to extend the results of [3] to the period 1870 –2017, and hence capture the "death" of the 1998 – 2014 hiatus. The regression model will be simpler than the one employed in [3], in the sense that the LRM temperature response to the sum of anthropogenic, volcanic, and solar forcing will be treated as one predictor, rather as three independent predictors. On the other hand, the LRM response to the ENSO and AMO indices are treated as predictors, rather than the indices themselves. This means that the number of predictors are reduced from five to three, and hence the chance of over-fitting is considerably reduced. This enhances the confidence we can

have in the model. In spite of the reduction of model complexity, the explained variance increases to 93%. This may be attributed to using the LRM-response to the ENSO index as predictor rather than the index itself, but updated and longer data sets may also play a role.

The forcing signals used as basis for the predictors are shown in Figure 1. Figure 1a displays the sum of volcanic, solar, and anthropogenic forcing, and Figure 1b those individual components of the forcing. Figures 1c and 1d display the AMO and the ENSO indices, respectively. Section 2.1 explains how these signals are filtered into signals that exhibit the temporal *fingerprints* of the GMST responses to these forcing signals. By means of a linear, multiple regression these fingerprints (or predictors) and the instrumental GMST are used to estimate regression coefficients which allow the formation of a weighted sum which represent the best fit to the instrumental data. Here each weighted fingerprint will be denoted the *footprint* of the specific forcing or index, since it can be interpreted as the component of that forcing or index present in the instrumental GMST.

The main results of this analysis are presented in Section 2 and further discussed in Section 3. The data sources are presented and some methodological issues further discussed in Section 4.
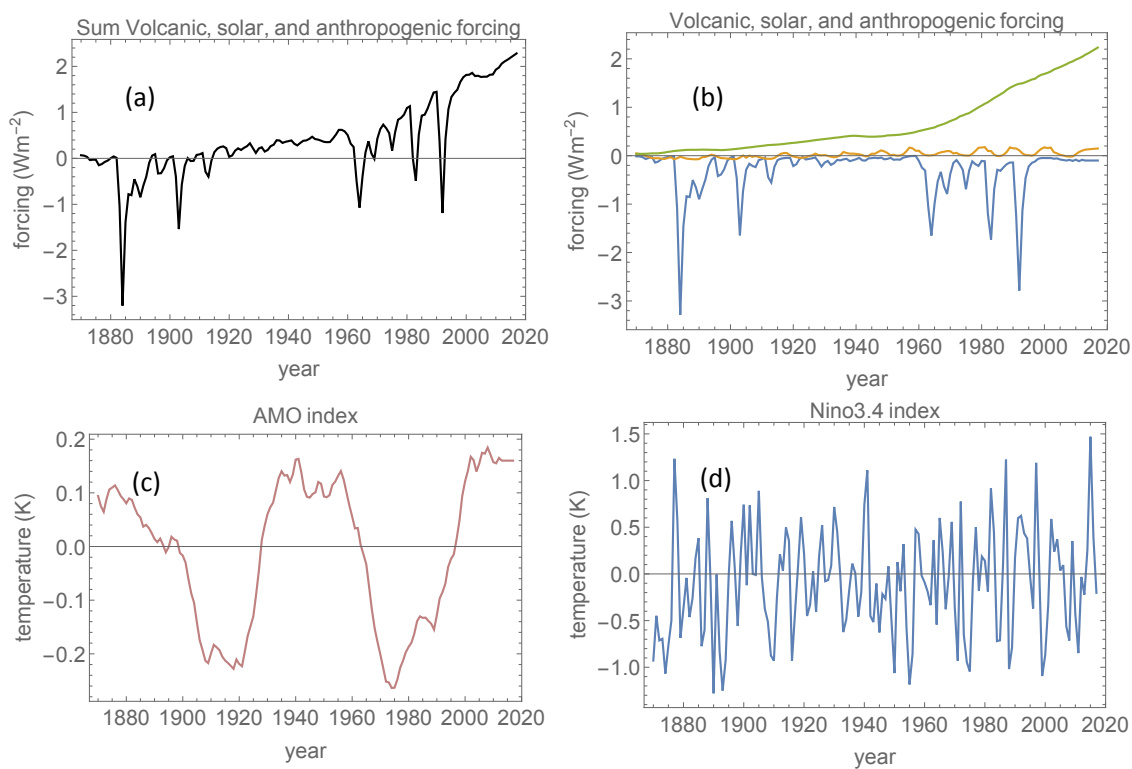

Figure 1. Forcing signals used in the regression analysis. (**a**) The sum of volcanic, solar and anthropogenic forcing. (**b**) Blue curve depicts the volcanic forcing, yellow curve the solar forcing and green curve the total anthropogenic forcing including greenhouse gases, land use change and anthropogenic aerosols. (**c**) The AMO index, and (**d**) the Niño3.4 index. These indices are not in units of forcing, but the correponding forcing is assumed to be proportional to the indices.

2. Results

2.1. Estimating the long-memory exponent for the GMST-response

If the GMST is supposed to respond linearly to radiative forcing $F(t)$ the general form of the response has the form of a convolution integral

$$T(t) = \int_0^t G(t - t') \left[F(t') + \sigma w(t') \right] dt', \tag{1}$$

where $T(t)$ is the temperature change relative to the time $t = 0$. Here, its is also added a stochastic forcing, where $w(t)$ is a Gaussian white-noise stochastic process. It is supposed to represent the random forcing on the GMST arising from atmospheric weather systems, but it is not a priori clear how to include distinct climatic modes like the AMO and ENSO in this description. It was shown by Rypdal and Rypdal (2014) [4] that by adding a white-noise forcing $\sigma w(t))$ to the known deterministic forcing $F(t)$, the residual internal variability (the climate noise) of $T(t)$ on time scales from years to centuries is well described by a response function of the power-law form

$$G(t) \sim t^{\beta/2-1}. \tag{2}$$

It can be shown that if $F(t) = 0$ the resulting internal variability would exhibit a power spectral density (PSD) on the form $S(f) \sim f^{-\beta}$. This property is called scale invariance, or simply *scaling*, because the statistical properties of the signal is independent of scale. Crudely stated, the signal looks the same if we zoom in or out. It was shown in [4] that this scaling is a feature of the residual climate noise of the instrumental GMST and it is also found in long control runs of atmospheric-ocean general circulation models [5]. In both cases the scaling seems to be reasonably valid on time scales from years to centuries with $\beta \approx 0.75$, although it has been recognized that that ENSO poses a problem to this picture [6].

The spectral exponent β measures the long-range memory (LRM) in the temperature signal; $\beta = 0$ corresponds to no memory (white noise), while $\beta = 1$ characterizes a "pink noise" process. For β in this range the stochastic process is a stationary persistent fractional Gaussian noise (fGn), while for $1 < \beta < 3$ it is a fractional Brownian motion (fBm), which is a non-stationary process.

This methodology includes internal modes like AMO and ENSO as part of the LRM climate noise. This may be problematic, since the PSDs of these modes peak in distinct frequency ranges and tend to break the scale invariance implied by the assumed scaling of the GMST signal. As a means to solve this problem, it is proposed here to include the AMO and ENSO in the deterministic forcing signal. These indices are not given in units of forcing, so the magnitudes of forcing they represent are not known. But this is unimportant, because it is only their temporal structure that is used in the regression. Their magnitude, and hence their footprints, are determined through the estimation of the regression coefficients.

A brief sketch of the the method of estimating β is given below. Details can be found in Section 4.2. The fingerprints of the deterministic forcing, AMO, and ENSO are found by convolving the forcing signal and the AMO and ENSO indices by the response function given by Eq. (2). The convolution has the form shown in Eq. (1). The three footprints contain multiplicative constants c_n, $n = 1, 2, 3$ which serve as regression coefficients in a linear multiple regression, where the fingerprints are the predictors. The exponent β is assumed to be the same for all fingerprints. By varying β in the range $0.3 - 0.9$ in steps of 0.1 the total footprint is computed for each β by regressing against the instrumental GMST, and the residual is computed by subtracting the footprint from the observed signal. The estimated scaling exponent $\hat{\beta}$ for the residual is then computed from the estimated PSD or from some other estimator. Here, the variogram estimator is used (see for instance Rypdal et al. (2013) [7] for definitions and discussion of various estimators). It measures how the variance of the cumulative sum of the signal depends on the time τ over which it is summed. If the signal is scale invariant this variance goes as a power-law $\tau^{\hat{H}}$, where $\hat{H}$ is the estimated Hurst exponent. The relation between $\hat{H}$ and $\hat{\beta}$ is $\hat{\beta} = 2\hat{H} - 1$ [7].
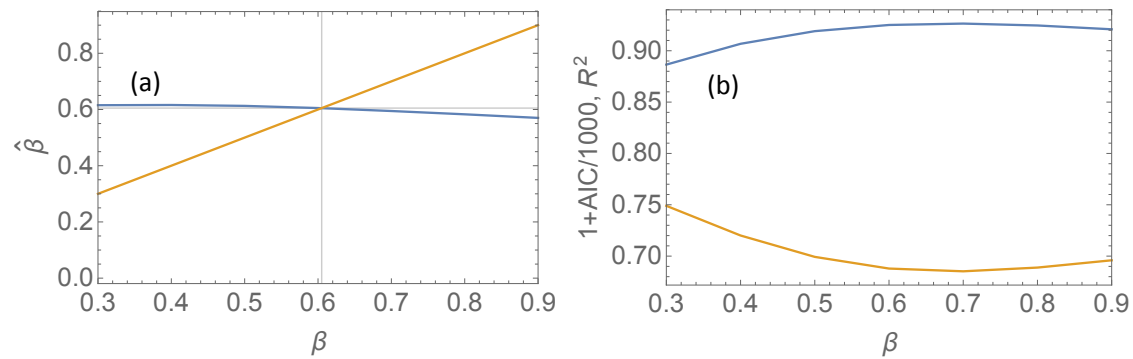
Figure 2. (**a**) The blue curve is $\hat{\beta}$ plotted against β estimated from the variogram of the residual signal obtained after regression using fingerprints obtained from filtering forcing signals by the response function $G(t) = ct^{\beta/2-1}$. The yellow curve is the straight line through the origin with unit slope. (**b**) The blue curve is R^2 of the regression plotted against β used in the response function. The yellow curve is $1 + AIC/1000$ versus β, where AIC is the Akaike information criterion.

In Figure 2a the blue curve depicts the estimate $\hat{\beta}$ versus the assumed β used in the response function, and the yellow curve is just the line through the origin with unit slope. The two curves intersect where $\hat{\beta} = \beta$, i.e. at the value $\beta \approx 0.6$ for which the response model is self-consistent. This value is a bit lower than the value $\hat{\beta} \approx 0.75$ estimated in [4], and should be considered as a correction due to the elimination of AMO and ENSO from the residual.

This result suggests that $\beta = 0.6$ is the preferred choice to use as a filter exponent to define the individual fingerprints. This choice is strengthened by computing the coefficient of explained variance R^2 (see [3]) against β. This is shown as the blue curve in Figure 2b, which peaks in the vicinity of this β-value. The yellow curve is a plot derived from the so-called Akaike information criterion (AIC) (what is plotted is $1 + AIC/1000$, see [3]). This criterion measures the explained variance with a penalty for model complexity. Of two statistical models, the one with the lower AIC is preferable to the other in an information-theoretical sense. The AIC curve has a minimum in the vicinity of $\beta = 0.6$ and hence supports this as the preferred value of the exponent in the subsequent analysis.
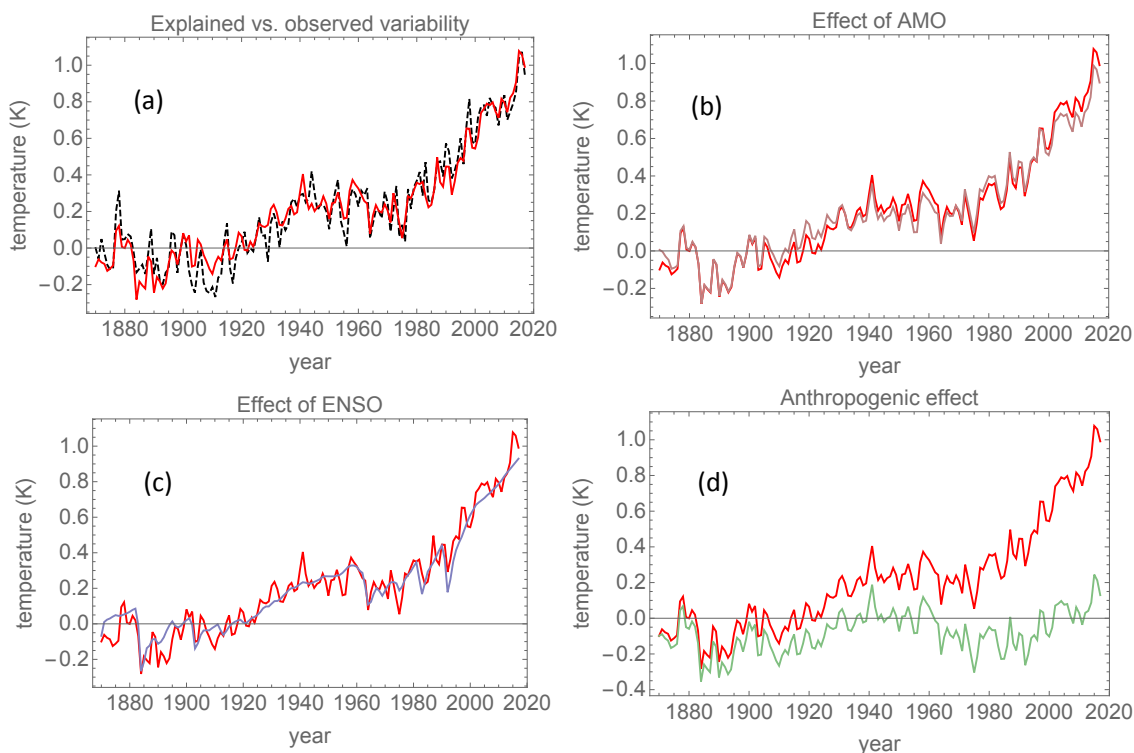
2.2. Instrumental GMST explained

Figure 3. In all four panels the red curve is the total explained GMST (or the total footprint) from the regression. (**a**) The black, dashed curve is the HadCrut4 GMST signal. (**b**) The brown curve is the signal obtained after the AMO-footprint has been subtracted from the total footprint. (**c**) The blue curve is the signal obtained after the ENSO-footprint has been subtracted from the total footprint. (**d**) The green curve is the signal obtained after the anthropogenic footprint has been subtracted from the total footprint.

Figure 3a shows the result of the regression analysis with $\beta = 0.6$, and with the fingerprints of deterministic forcing, AMO, and ENSO used as predictors. The regression determines the three coefficients c_1, c_2, c_3 and the total footprint (the red curve) explains 92.5% of the variance of the observed GMST (the black, dashed curve). One observes that the three pauses discussed in Section 1 are all explained by the superposition of these three footprints.

One would perhaps have expected that the AMO explains a considerable part of the two first pauses and part of the most recent hiatus, but the effect of AMO is in fact quite small. This is seen in Figure 3b, where the total footprint (red) is plotted along with the signal obtained with the AMO-footprint subtracted (brown). The two first pauses give the graph of the entire time series an appearance of a slow oscillation more or less in phase with the AMO and superposed on a rising trend, but this oscillation is not created by the AMO. It is caused by the clustered structure of the volcanic forcing, one cluster in the interval 1880 – 1920 CE, and another in the interval 1960 – 2000 CE. Actually, this phase coincidence suggests that the AMO may be paced by this clustering. This assertion is supported by repeating the analysis without using the AMO as a predictor. The results are not substantially different, and are not shown here.

In Figure 3c the blue curve shows the total footprint with the ENSO-footprint subtracted. As expected, the two first pauses are not substantially altered by removing the effect of ENSO, but the most recent hiatus essentially disappears. After subtracting the effect of ENSO, the negative spikes caused by volcanic eruptions appear much more clearly. This shows that volcanic and ENSO footprints are of comparable magnitude and operate on the same time scales.

The anthropogenic influence is demonstrated explicitly in In Figure 3d, where the green curve is the total footprint with the anthropogenic footprint subtracted. This green curve is the natural footprint comprised of the footprints of volcanic and solar forcing with a weak contribution from AMO and a strong contribution from ENSO (see Figure 1). The slow oscillation with period around 60 years is mainly caused by the clustering of volcanic eruptions, the fast annual to decadal scale fluctuations are a combination of fast responses to volcanic eruptions and ENSO, with a weak contribution from the 11-year solar cycle.

2.3. The recent hiatus and warming trend

Figure 4a is a close-up on Figure 3a for the period 1970 – 2017, and Figure 4b is a close-up of Figure 3c. The red, dashed line is a linear fit to the total footprint (the red, full curve), and the slope corresponds to 0.182 K per decade. The blue, full curve in Figure 3b shows that as the effect of ENSO is removed, the actual temperature rise during 2000 – 2017 follows the linear-fit line to this curve for the period 1970 – 2017, which has the slope 0.166 K per decade. Thus, with ENSO-footprint included the variability of this period is very accurately explained, including the hiatus. When ENSO is removed, the hiatus disappears and what remains is a linearly growing trend on which we observe the effect of three volcanic eruptions prior to the turn of the century. During the hiatus period, the hiatus is completely replaced by this linear trend when ENSO is removed, so we can conclude that the 1998-2015 hiatus, and its death during the years 1916-2017, is first and foremost an effect of ENSO.
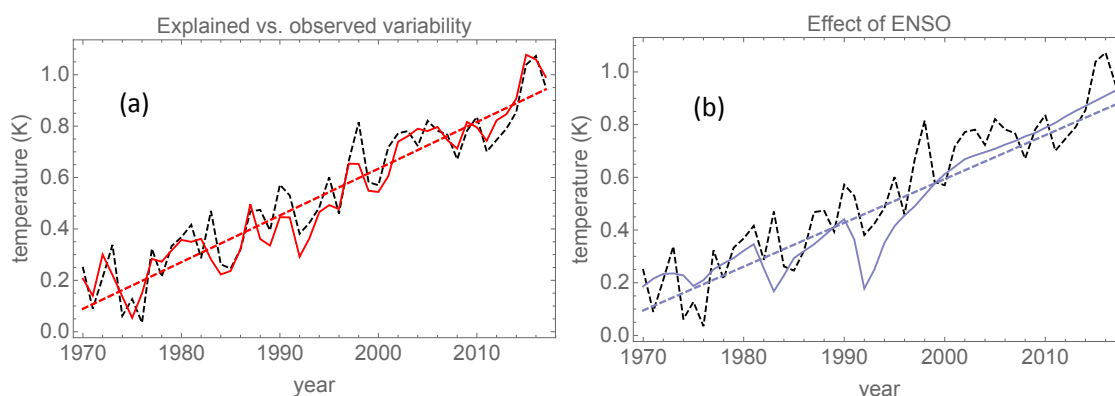

Figure 4. (**a**) A close-up on Figure 3a. The red, dashed line is a linear fit to the red curve. (**b**) A close-up on Figure 3c. The blue, dashed line is a linear fit to the blue curve.

3. Discussion

Rypdal (2015) [3] obtained R^2 (89%) slightly smaller than obtained here (92.5%) by using volcanic, solar, and anthropogenic fingerprints as independent predictors in addition to AMO and ENSO. In other words, in that paper five predictors gave no better results than we obtained here with three. On the other hand the AIC found there was -244, while the present analysis found AIC=-312 due to the reduced model complexity. One of the major differences in these two analyses is that in [3] the volcanic footprint was reduced by a 41% while the AMO footprint was stronger. A plausible interpretation of this difference is that the freedom of allowing different effective sensitivities to the volcanic, solar, and anthropogenic forcing components results in unphysical over-fitting. The situation is complex, however, since a number of other factors are different in these analyses. For instance, the data series in the present work are longer (1870 – 2017 versus 1880 – 2010), and both the GMST time series and the forcing time series have been updated. From an information-theoretical viewpoint the present analysis is preferable, and the data used are likely more correct. The reduced AMO-footprint has the interesting implication that the slow oscillation of period of about 60 years, giving rise to the pauses 1870 – 1915, 1940 – 1970, can be attributed to the clustering of volcanic

eruptions. Moreover, since the phase of AMO coincides with this oscillation, it opens the possibility that AMO during the 20th century was paced by the volcanic activity.

Another conclusion that can be drawn from comparing these results with those obtained by Lean and Rind (2008) [2], and by Rypdal (2015) [3] using a zero-memory (instantaneous) response function, is that a long-memory response is required to fully reproduce this slow oscillation as a response to the clustering of volcanic activity. Hence, it serves as a confirmation of the usefulness of the long-memory response description and emphasizes that volcanic forcing has effects not only a few years after eruptions but also on multi-decadal time scales (see also Figure 5 and the discussion in Section 4.2).

By including AMO and ENSO as a part of the deterministic forcing, and hence excluding these signals from the residual climate noise background, the present work obtains a better scaling description of this background on time scales from years to a few decades, and a memory exponent of $\beta \approx 0.6$ (corresponding to a Hurst exponent of $H = 0.8$) has been obtained. This eliminates a problem that plagues many studies where ENSO creates difficulties for computing scaling exponents (see e.g. Fredriksen and Rypdal (2016) [6]).

Seen in the context of the entire instrumental 1870 – 2017 GMST record, the most remarkable feature of the the 1998 – 2015 hiatus is how unremarkable it is. The duration of the period with zero GMST trend is considerably shorter than those of the pauses 1870 – 1915, 1940 – 1970, during which the trends were actually not zero, but negative. There have been no strong volcanic eruptions since the Mount Pinatubo eruption of 1993, but a particularly deep solar minimum in 2009 and a the weak solar cycle 24 during the following decade lead to the dip in the total forcing during the first decade of this century observed in Figure 1a. By first sight this might suggest that the entire hiatus could be attributed to this low solar forcing, but it is not supported by Figure 4b where elimination of the ENSO footprint also essentially eliminates the hiatus. On the other hand, the solar footprint may explain the slightly higher slope of the trend line in Figure 4a (0.182 K per decade) compared to 0.166 K per decade in Figure 4b. Figure 3b and Figure 5d show that AMO is responsible for a positive temperature anomaly of about 0.1 K during the interval 2000 – 2017, but this perturbation is almost constant during the period and does not significantly influence the shape of the hiatus. The overall conclusion is that the 1998 – 2015 hiatus is an unremarkable phenomenon that can be attributed to the influence of ENSO on the global mean surface temperature, with a slightly reduced warming trend due to low solar activity.

4. Materials and Methods

4.1. Data

The GMST data used in this paper is the HadCrut4 global temperature time series [8], data available at;
https://crudata.uea.ac.uk/cru/data/temperature/HadCRUT4-gl.dat

The forcing data is an updated version of [9], data available at;
http://www.columbia.edu/m̃hs119/Forcings/

This data series goes to 2015. The two last data points for 2017 and 2016 used in the analysis have been obtained by linear extrapolation.

The AMO-index data is the AMO smoothed, long time series derived from the Kaplan SST data set [10], data availble at;
https://www.esrl.noaa.gov/psd/data/timeseries/AMO/

The Nino3.4 index is described in [11], data available at;
https://www.esrl.noaa.gov/psd/data/correlation/nina34.data

4.2. Methods

Let $F_1(t)$ be the total forcing signal plotted in Figure 1a, $F_2(t)$ the AMO-index in Figure 1c, and $F_3(t)$ the Nino3.4-index in Figure 1d. The predictors corresponding to these signals are the filtered functions $\mathcal{F}_n(t) = \int_0^t (t-t')^{\beta/2-1} F_n(t')\,dt'$, $n = 1, 2, 3$, $\beta = 0.6$, which may be perceived as the *fingerprints* of the signals $F_n(t)$ to be detected in the GMST response. The *response function* (or the *predictand*) is the linear combination

$$Q(t) = c_0 + \sum_{n=1}^{3} c_n \mathcal{F}_n(t). \tag{3}$$

The multiple, linear regression determines the regression coefficients c_n, $n = 0, 1, 2, 3$ that minimize the square deviation between $Q(t)$ and the observed GMST.

The regression coefficients are obtained by the command *LinearModelFit* in *Mathematica*. For selection of the optimal β we computed for each $Q_\beta(t)$ the R^2 diagnostic (*coefficient of determination*), which measures the fraction of the total variance in the observed record that is explained by the predictand. In model selection assessments we have model selection criteria based on information theory where the likelihood function is used as a measure of the goodness of the fit, which is subject to a penalty for model complexity. The most commonly used of these are the Akaike information criterion (*AIC*) [12]. This criterion produces a real number that can be positive or negative, and the model giving the smaller number is in this particular sense preferable. These diagnostics are directly available as options in *LinearModelFit*.
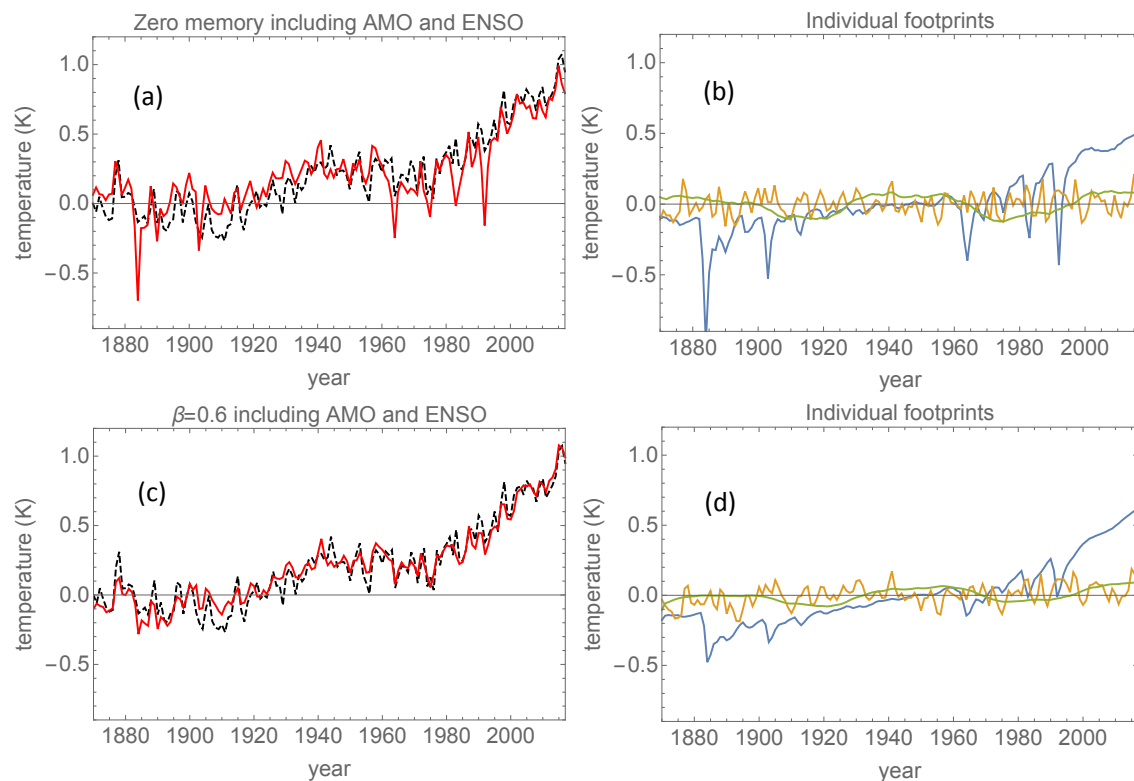

Figure 5. (**a**) The red curve is the total explained GMST (or the total footprint) from the regression when the fingerprints are the unfiltered forcing and indices. The black, dashed curve is the HadCrut4 GMST signal. (**b**) The individual footprints whose sum is the red curve in panel (**a**). The blue curve is the volcanic, the yellow curve the ENSO, and the green curve the AMO footprints, respectively. (**c**) and (**d**) The same as panels (**a**) and (**c**) with fingerprints filtered with $\beta = 0.6$.

The main effect of the LRM filtering is to smear out the responses to forcing features that are localized in time, such as volcanic eruptions and ENSO-events, but it also causes some redistribution of the weights that are given to slower features such as the AMO footprint versus the volcanic footprint. This is illustrated in Figure 5. In Figure 5a,b the regression has been done without any filtering of the forcing signals, i.e. the fingerprints that are used as predictors are the forcing signal and the AMO and ENSO indices themselves. In Figures 5c,d the fingerprints are the forcing and indices smoothed with the $\beta = 0.6$ filter. Figure 5a compared to Figure 5c shows that the lack of filtering yields too strong short-time responses to the volcanic eruptions. This appears even more clearly when Figure 5b is compared to Figure 5d. Here, the individual footprints of the total forcing and the indices are plotted to show their relative strength.

The LRM filtering results in a somewhat weaker AMO footprint, but the slow 60-year period oscillation is reproduced equally well in Figure 5a and 5c. This is because the weaker AMO footprint is compensated by a slow response to the clustering of the volcanic eruptions which produces a similar oscillation.

Conflicts of Interest: The author declares no conflict of interest.

References

1. Foster, G.; Rahmstorf, S. Global temperature evolution 1979–2010, *Environ. Res. Lett.* **2011**, *6*, 044022.
2. Lean, J. L.; Rind, D. H. How natural and anthropogenic influences alter global and regional surface temperatures: 1889 to 2006. *Geophys. Res. Lett.* **2008**, *35*, L18701.
3. Rypdal, K. Attribution in the presence of a long-memory climate response. *Earth Syst. Dynam.* **2015**, *6*, 719-730.
4. Rypdal, M.; Rypdal K. Long-memory effects in linear-response models of Earth's temperature and implications for future global warming. *J. Climate* **2014**, *27*, 5240-5258.
5. Østvand, L.; Nilsen, T.; Rypdal, K.; Divine, D.; Rypdal, M. Long-range memory in internal and forced dynamics of millennium-long climate model simulation. *Earth. Syst. Dynam.* **2014**, *5*, 295-308.
6. Fredriksen, H-. B.; Rypdal, K. Spectral characteristics of instrumental and climate model surface temperatures. *J. Climate* **2016**, *29*, 1253-1268.
7. Rypdal, K.; Østvand, L.; and Rypdal, M. Long-range memory in Earth's surface temperature on time scales from months to centuries. *J. Geophys. Res.* **2013**, *118*, 7046-7062.
8. Morice, C. P.; Kennedy,J. J.; Rayner,N. A.; Jones,P. D. Quantifying uncertainties in global and regional temperature change using an ensemble of observational estimates: The HadCRUT4 dataset. *J. Geophys. Res.* **2012**, *117*, D08101.
9. Hansen, J.; Sato, M.; Kharecha, P.; von Schuckmann,K.: Earth's energy imbalance and implications. *Atmos. Chem. Phys.* **2011**, *11*, 13421–1344.
10. Kaplan, A.; Cane, M.; Kushnir, Y.; Clement, A.; Blumenthal, M.; Rajagopalan, B. Analyses of global sea surface temperature 1856-1991. *Journal of Geophysical Research* **1998**, *103*, 18567-18589.
11. Trenberth, K. E. The Definition of El Niño. *Bulletin of the American Meteorological Society* **1997**, *78*, 2771-2777.
12. Burnham, K. P.; Anderson, D. R. Multimodel inference: understanding AIC and BIC in model selection. *Sociological Methods & Research* **2004**, *33*, 261-304.